
Article:
Zhang, W., Li, G.-J. orcid.org/0000-0002-5956-4033 and Qin, Y. (2024) Comparative study of ferrofluid cooling for permanent magnet machines with different winding structures. IEEE Access. ISSN 2169-3536

https://doi.org/10.1109/ACCESS.2024.3359900

IEEE Access
Multidisciplinary | Rapid Review | Open Access Journal

Date of publication xxxx 00, 0000, date of current version xxxx 00, 0000.

Digital Object Identifier xxx

Comparative Study of Ferrofluid Cooling for Permanent Magnet Machines with Different Winding Structures

W. Zhang, G. J. Li, Senior Member, IEEE, Y. Qin

Department of Electronic and Electrical Engineering, The University of Sheffield, Sheffield, UK,

Corresponding author: Guang-Jin Li (e-mail: g.li@sheffield.ac.uk).

This work is supported by the UK Engineering and Physical Science Research Council (EPSRC) under Grant No. EP/T017988/1.

ABSTRACT This paper investigates the influence of single- and double-layer winding structures on the thermal performances of fractional slot permanent magnet (PM) machines with ferrofluid cooling. Ferrofluid is an oil-based liquid with nano-sized ferromagnetic particles and has been injected into the end space of these machines. Owing to the magnetic body force produced by the end-winding leakage flux, the ferrofluid can circulate without the need for external pumps. This enables the establishment of an effective heat transfer path from the end-windings to the housing with water jacket. As a result, the ferrofluid improves the heat transfer rate and hence machine's overall thermal performance. Multiphysics models accounting for the coupling between electromagnetic (EM) field, fluid dynamics and heat transfer have been built for the investigations. In addition to the dc field simulation as that carried out in literature, these multi-physics models can also simulate the effect of ac field in the end space. The findings indicate that ferrofluid cooling significantly improves the EM and thermal performances for the fractional slot PM machines. In addition, due to different magnetic fields in the end space produced by the single- and double-layer windings, they exhibit different cooling efficiencies. A motorette has been built to validate the simulations.

INDEX TERMS Ferrofluid cooling, magnetic body force, single/double layer winding, thermomagnetic effect.

I. INTRODUCTION

Permanent magnet (PM) machines have attracted increasing interest in a wide range of industry applications including automotive, renewable energy and aerospace due to their high torque/power density and high efficiency. However, because of the use of rare-earth PMs, e.g., NdFeB or SmCo, the costs of these PM machines are generally higher than other magnet free machines like induction machines and switched/synchronous reluctance machines. In addition, under elevated operating temperature, PMs are prone to irreversible demagnetization, which is a partial loss of energy density that could lead to significantly deteriorated electromagnetic (EM) performance. To avoid magnet irreversible demagnetization for high power density applications, it is essential to keep the magnet temperature within a maximum allowable range. This can be achieved by using advanced thermal management, which is also vital for windings as according to the Montsinger law, a 8℃ to 10 ℃ temperature rise above the allowable operating temperature can halve the life span of winding insulation [1].

There are different thermal management strategies that can be employed to improve machines' thermal performance. This includes natural air/liquid cooling, forced air/liquid cooling and radiation cooling [2]. Cooling fins, usually on the housing surface, is one of the most widely used natural cooling technologies which increases the heat exchange surface area on the machine housing [3]. This is a simple and relatively effective way of reducing the overall temperature within the machines. However, because it uses air as cooling medium, the achievable cooling efficiency is often limited. To achieve better cooling efficiency, forced liquid cooling technologies such as water jacket [4, 5] and shaft cooling [6, 7] can significantly improve the heat transfer rate and hence become more and more popular for high power density applications. It is worth noting that these cooling technologies are effective in removing heat from the machine active parts, i.e., active windings in stator slots and rotor magnets. However, they are much less effective in reducing the end-winding temperatures, leading to the hot spot being in the end-windings. This is mainly due to the poor thermal conductivity of air in the end space and therefore a high thermal resistance between the end-windings and machine housing where cooling system such as water jacket is located. To improve the cooling of end-windings, ventilation cooling [8, 9] and forced oil cooling [10, 11] have been investigated. For these cooling technologies, inlets and outlets are introduced on the endcaps or machine housing to allow air or liquid to flow through the machine. This has been found to be able to significantly reduce the end-windings temperature. However, for the above cooling technologies, the forced oil cooling in particular, the end-windings and other machine components are directly exposed to the high-speed coolants. This can accelerate the insulation degradation. In addition, hollow conductors with coolant circulating inside them can also be used to achieve excellent winding cooling efficiency [12]. However, such cooling method is not very suitable for small and medium sized electrical machines due to relatively small conductor sizes. Self-circulating cooling, such as rotor or shaft mounted fan [13, 14], can establish an effective heat transfer path between the end-windings and the housing, and hence becomes more and more popular. For such cooling method, the fans are driven by the rotor, so the cooling efficiency is fairly limited at low speed high torque conditions. To address this issue, some new materials with high thermal conductivities, e.g., transformer oils or potting materials, are used to fill in the end space [15, 16]. The thermal conductivities of these materials are often several times higher than air, so they can significantly reduce

the thermal resistance between the end-windings and the machine housing.

In recent years, an advanced cooling technology using ferrofluid (FF) materials has gained increasing interest first in cooling for power electronics devices [17] and transformers [18-20], then in cooling for electrical machines [21, 22]. The findings in literature have shown that ferrofluid cooling has been effective in reducing the temperature of these devices. This is because ferrofluid can subject to the magnetic body force in the presence of magnetic field gradients or discontinuities [23]. It results in a self-circulation of the liquid, which improves the heat transfer rate. This phenomenon is known as thermomagnetic convection or the thermomagnetic effect [24, 25].

For ferrofluid cooling, it is also found that the variation of magnetic field can directly affect the magnetic body force, therefore the efficiency of thermomagnetic convection. As for the electrical machines with different winding configurations, e.g., single- and double-layer windings, they will have different end-winding leakage fluxes. This would lead to different cooling performances when the ferrofluid cooling is employed. To investigate the impact of winding configurations on the cooling efficiency of machines with ferrofluid cooing, in this paper, multiphysics models using COMSOL software package will be developed, as shown in Fig. 1. These multiphysics models are necessary because a strong coupling between EM, heat transfer and fluid dynamics will be required to accurately predict the performances of ferrofluid cooling. It is worth noting that, a water jacket is also adopted for cooling the machines. This is because even if the ferrofluid cooling is a passive cooling method that does not require extra pump to drive the coolant, it can only establish an effective heat transfer path between the end-windings and the housing. Without a water jacket or other types of forced air/liquid cooling, its efficiency will be limited by the poor convection on machine surfaces and its full potential cannot be achieved.

Moreover, two different simulation models are developed in this paper as detailed in Appendix. The influence of rotating magnetic field for the electrical machines will be investigated by comparing these two models.

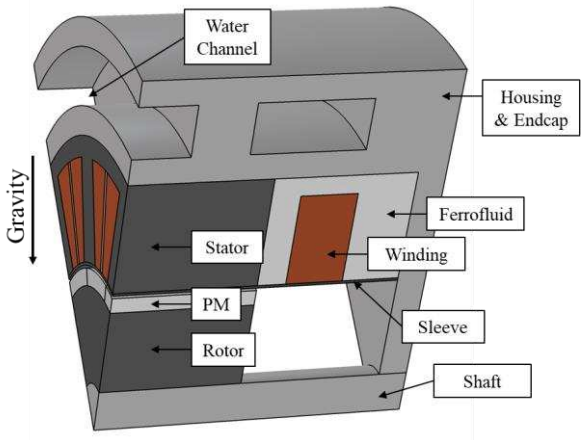

Fig. 1. PM machine with ferrofluid (around end-winding) and water jacket.

II. THEORETICAL BACKGROUND OF FERROFLUID

The ferromagnetic nanoparticles in ferrofluid can be magnetized by external magnetic field. The magnetization increases with the increasing magnetic field strength until it reaches the saturation. It is worth noting that, since the ferrofluid is placed under a relatively weak magnetic field that Langevin argument (ξ) is much smaller than 1, the magnetization (M) of ferrofluid is assumed to be linearly proportional to the magnetic field strength (H), such as

$$M = \chi H \tag{1}$$

where χ is the magnetic susceptibility and is temperature dependent. By approximating the Langevin function, χ of ferrofluid is given as

$$\chi = \frac{\phi \mu_0 \pi d^3 M_{s,p}(T)^2}{18 k_B T} \tag{2}$$

where μ_0 is the vacuum permeability, ϕ is the volume fraction, d is the average diameter of ferromagnetic particles, k_B is the Boltzmann constant, T is the absolute temperature and $M_{s,p}(T)$ is the temperature dependent saturation magnetization.

The magnetic body force is one of the most important components in the multiphysics modelling of ferrofluid cooling. There are several models developed in literature to calculate the magnetic body force, including the electrical current loop model, the magnetic charge model, and the Kelvin body force formula [23, 26-29]. Amongst all these models, the Kelvin body force formula [see (3)] is the most widely used in literature. This model neglects the interaction between the nano-sized ferromagnetic particles in the ferrofluid, therefore, it can simplify the simulations.

$$\boldsymbol{F_m} = \mu_0 (\boldsymbol{M} \cdot \boldsymbol{\nabla}) \boldsymbol{H} \tag{3}$$

where $\boldsymbol{F_m}$ is the magnetic body force vector.

An accurate ferrofluid model requires an accurate magnetic field because the magnetic body force is affected by it as described by (3). For the models of PM machines investigated in this paper, the magnetic field is generated by 3-phase alternating currents (AC). However, if AC currents are used, the multiphysics models considering the coupling between EM and fluid dynamics will be excessively time-consuming. This is mainly because the electrical time constant (a few ms) is much shorter than the hydrodynamics and thermal time constants. Using AC currents means a time step of ms level would be needed in the model to maintain any meaningful accuracy. This will significantly increase the computation time and could even make the models unsolvable. To address this issue, in most existing studies [18-20, 25], a quasi-steady magnetic field generated by direct current (DC) that has the same value as the rms value of the AC current is used to generate a similar magnetic field. This model (named as model 1) is accurate enough for transformers or electrical machines with coils that are relatively far apart, such as single layer machines [22]. In these machines, the magnetic field in the end space is mostly generated by each coil itself with little mutual flux from adjacent coils. More details can be seen in Appendix A. However, when the coil number is increased and the distance between adjacent coils is reduced, such as the case of a double layer machine, the magnetic field at each location within the end space will be generated by more than one coil. Therefore, a DC current will not be able to fully represent the real AC current. To overcome this problem, a new model (model 2) should be introduced. More details can be seen in Appendix B.

The properties of the ferrofluid that will be used for the investigations in this paper are listed in Table I. It is worth noting that the temperature dependent viscosity will be introduced in the model, where it is described by Andrade's equation [30] as

$$\eta = Ae^{\frac{B}{T}} \tag{4}$$

where coefficients A and B are the characteristics of ferrofluid and can be obtained from empirical parameters. In this paper, $A = 1.3 \times 10^{-6}$ Pa · s and $B = 3.1 \times 10^{3}$ K.

It is worth noting that, the specific heat capacity of materials can also affect the thermal steady state. However, since the volume fraction is small, the difference of specific heat capacity between ferrofluid, oil and nanofluid id negligible. Moreover, the electrical resistivity of ferrofluid is larger than $10^{9}\Omega$m and the induced current within the ferrofluid is neglected.

TABLE I PARAMETERS OF THE FERROFLUID

Volume fraction (%)	5.4	Curie Temperature (K)	793
Saturation magnetization at 20℃ (kA/m)	387	Specific heat capacity (J/kg/K)	1685
Thermal expansion ($\times 10^{-4}$ 1/K)	6.62	Thermal conductivity (W/m · K)	0.186
Density (kg/m^3)	1115	Dynamic viscosity (Pa · s)	0.0787

III. MULTIPHYSICS MODELLING

A. Machine Features and Specifications

Two typical fractional slot surface-mounted PM (SPM) machines with single- and double-layer windings, as shown in Fig. 2, have been compared in this paper. This will allow us to study the influence of winding structures on the cooling performances of ferrofluid. For a fairer comparison, only the winding structures are different, and all the other key design parameters are the same, as listed in TABLE II. It is also worth noting that, the number of turns per coil of the double layer machine is half of that of the single layer machine. However, as the number of coils of the double layer machine is twice that of the single layer machine, both machines have the same total number of turns per slot. This leads to the same current density for these two winding topologies.

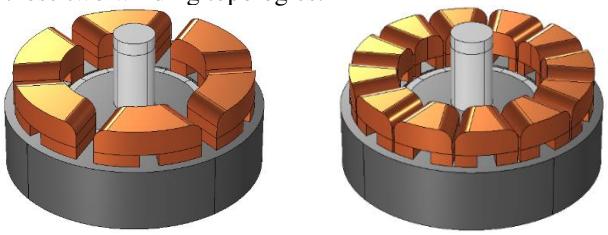

(a) (b)

Fig. 2. Views of end-windings for (a) single- and (b) double-layer windings.

TABLE II PARAMETERS OF THE SPM MACHINE

Slot number	12	Stack length (mm)	50
Pole number	14	End-winding overhang (mm)	15
Stator outer radius (mm)	50	Housing radius (mm)	65
Stator yoke height (mm)	3.7	Housing length (mm)	120
Tooth width (mm)	7.1	Nº of turns per phase	132
Airgap length (mm)	1	Wire diameter (mm)	1.32
Rotor outer radius (mm)	27.5	Current density (A/mm^2)	18.4
Magnet thickness (mm)	3		

B. 3D Multiphysics Modelling

To fully take advantage of the ferrofluid cooling, a water jacket embedded in the housing wrapping the stator iron core is introduced. The water jacket has been extended to cover the machine end-windings. This is to remove the heat generated in the end-windings by ferrofluid, as shown in Fig. 1. Without the water jacket or similar effective cooling technologies, even if an effective heat transfer path can be established between the end-windings and the housing via ferrofluid, the overall machine thermal performance is very much limited. Based on the simulation results, this water jacket can provide a convection coefficient of 3718 W/m^2/K at the housing surface when the total pressure drop for the water jacket is around 1200 Pa. The 3D multiphysics models are built using COMSOL Multiphysics 5.6. It is worth noting that, the gravitational effect plays an important role in the ferrofluid cooling in this paper. Therefore, it is considered in the multiphysics models, and its direction is vertical to the rotor shaft as shown in Fig. 1 as the machines are assumed to be placed horizontally. It is found that the horizontally placed machine (with water jacket) has better cooling performance than vertically placed machine. This is because a coolant circulation between the housing and the end-winding are well established for horizontally placed machine. However, for the vertically placed machine, the main coolant circulation established by gravity is between the endcaps (without water jacket) and the end-windings. The much lower thermal convection (20 W/m^2/K) on the endcaps leads to a poorer overall thermal performance of the vertically placed machine.

In order to show the superior cooling performance of ferrofluid, air and non-magnetic liquid, i.e., nanofluid (NF), have also been investigated, and compared against the ferrofluid cooling. Nanofluid has the same physical properties as ferrofluid but will not experience magnetic body force from the external magnetic field. This comparison will help investigate the influences of thermomagnetic convection and gravitational effect on ferrofluid cooling. To visualize the coolant behaviour of different coolants in different winding designs, two planes as shown in Fig. 3, one is vertical (plane 1) and the other is horizontal (plane 2) to the shaft, are used to show the temperature distribution and fluid flow in the following sections.

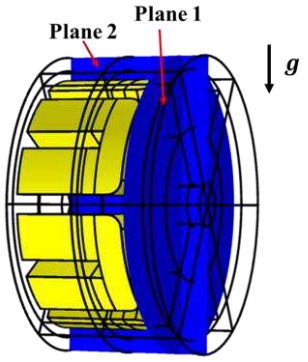

Fig. 3. Planes chosen to show the temperature distribution and fluid flow. *g* represents the gravity.

C. Air and Nanofluid Cooling

Firstly, at rated condition, when both the investigated machines only have air in the end space, the maximum end-winding temperature for the single layer machine is 151℃, while for the double layer machine it is 158℃. Higher machine temperature for the double layer machine is mainly because an extra insulation paper should be used to separate the different

coils in the same slot. This not only reduces the contact surface between the coils and stator, but also introduces extra thermal resistance between the coils. Even if the surface area of the end-winding for the double layer design is 38% higher than that of the single layer design, the poor thermal conductivity of air cannot fully utilize this advantage.

However, when a nanofluid is used to fill in the end-winding region, the thermal performance for the double layer machine can be significantly improved. For the single layer topology, using nanofluid in the end space reduces 5℃ of the maximum end-winding temperature (from 151℃ to 146℃). However, for the double layer topology, the maximum end-winding temperature is reduced by 17℃ (from 158℃ to 141℃). Since the winding losses for both designs are similar, the gravitational effect for both winding designs is almost the same. Therefore, the coolant velocities are similar as shown in Fig. 4 and hence the impact on the cooling efficiency due to the gravitational effect is similar too. However, for the double layer machine, the surface area of the end-windings is higher than that of single layer machine. In addition, the number of turns per coils is only half of that of the single layer machine. Therefore, the heat flux path from the hot spot (often at the centre of coils) to the surface is shorter than the single layer machine. As a result, the end-windings of the double layer machine can benefit more from the nanofluid cooling and hence have lower peak temperature.

The gravitational effect will be more significant when current density increases for both machines, as shown in Fig. 5. For the single layer machine, the temperature reduction (using nanofluid to replace air in the end-space) increases from 5℃ to 12℃ when the current density increases from 18.4A/mm^2 to 22.1A/mm^2. Similarly, for the double layer machine, this temperature reduction also improves from 17℃ to 31℃.

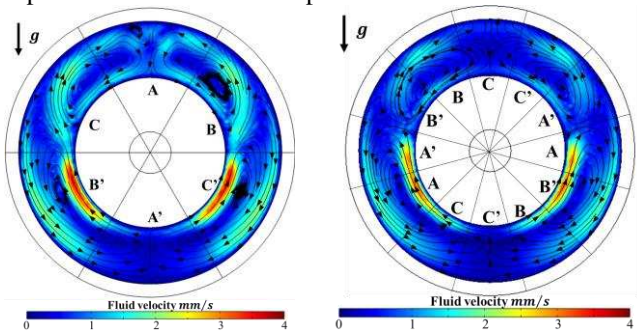

(a) (b)

Fig. 4. Fluid flow velocity at plane 1 for (a) single layer machine and (b) double layer machine with nanofluid cooling systems.

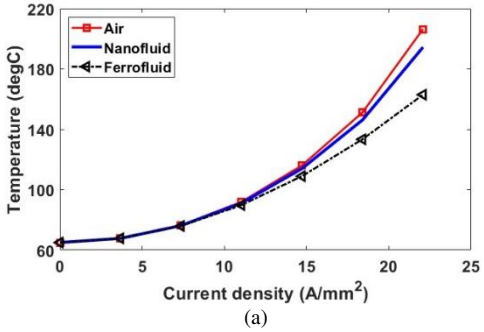

(a)

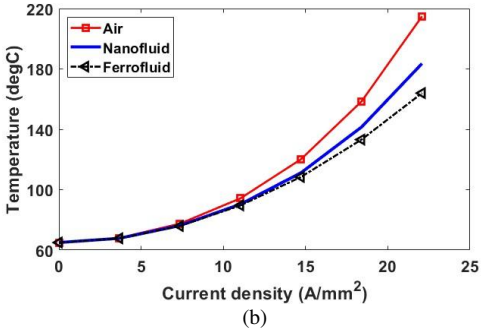

(b)

Fig. 5. Steady-state peak coil temperatures *vs* current density for different coolants in the end-space. (a) Single layer and (b) double layer machines.

D. Ferrofluid Cooling

Two types of models, i.e., model 1 and model 2 as described in Appendix A and B, have been introduced to investigate the ferrofluid cooling performances of both SPM machines. The maximum winding temperatures of these two winding topologies have been compared, as shown in Fig. 6.

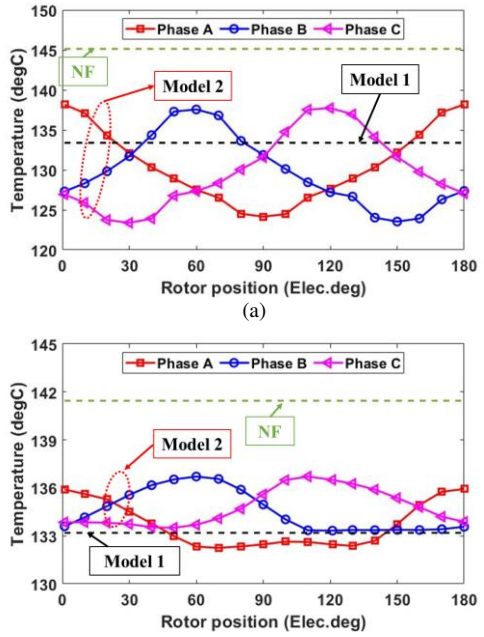

(a)

(b)

Fig. 6. Maximum coil temperature of each phase for (a) single layer machine and (b) double layer machine.

a. Single layer windings

For the single layer topology [as shown in Fig. 6 (a)], when the ferrofluid cooling is introduced to replace NF, a significant reduction of end-winding temperature can be achieved. This is validated by the results obtained from both model 1 and model 2. In model 1, the maximum winding temperature is 133℃ as shown by the black dashed line. However, in model 2, the peak winding temperature of each phase exhibits a periodical quasi-sinewave variation. Comparing with the phase currents at different rotor positions (see Fig. 7), the peak temperature of each phase is almost inversely proportional to the absolute value of the current injected to the corresponding phase. This is because higher current generates higher magnetic field strength, and hence better thermomagnetic convection. As the copper loss (heat source) is assumed to be the same and constant at different rotor positions (see Appendix B for more detailed

explanations), better thermomagnetic convection will mean more efficient heat removal from the end-windings.

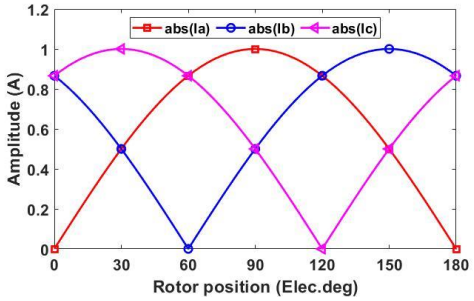

Fig. 7. Absolute value of current in each phase *vs* rotor position.

As the peak temperature of each phase obtained by model 2 varies periodically with rotor position, an average value of 131℃ of these peak temperatures for 180 Elec. Deg. is used to approximate the real peak temperature of each winding. This is deemed to be the closest to the case where real AC currents are supplied to the machine windings. Compared to model 1, model 2 would be more accurate but its computation time could be 10 times longer. However, the difference of winding temperature obtained by models 1 and 2 is only 1.5%, and hence not significant. This is because, for the single layer design, the magnetic field in the end-winding region is mainly generated by each end-winding itself and not affected by adjacent end-windings. This fact is also demonstrated by the coolant velocity distributions, as shown in Fig. 9 (a) and (b). The coolant close to coils reaches high coolant velocity for both models and the value of velocity is similar. However, the coolant velocity located between the two adjacent coils has been underestimated by model 1. It results from the underestimation of $\boldsymbol{K}_{(R)}$ in (15). $\boldsymbol{K}_{(R)}$ is assumed to be 1 for model 1, but it is actually much larger than 1 in the region that is around the centre of two adjacent coils. More details can be found in Appendix A.

The results obtained from both models 1 and 2 point towards the fact that the thermomagnetic convection is efficient for machine cooling. The temperature differences between nanofluid and ferrofluid cooling systems are 13℃ (for model 1) and 15℃ (for model 2). This is mainly due to the magnetic body force exerting on the ferromagnetic particles in the ferrofluid that increases the fluid circulation, and hence contributes to better cooling effect. This cooling effect will be more pronounced when higher electrical loading (or current density) is injected, as shown in Fig. 5 (a). According to (11), increasing the electrical loading improves the magnetic body force, and hence the thermomagnetic effect. As a result, the temperature reduction using ferrofluid to replace nanofluid is increased from 13 ℃ to 31 ℃ when the the current density increases from 18.4A/mm^2 to 22.1A/mm^2.

The average convection coefficients at endwinding surfaces for single layer machine with different cooling methods are shown in Fig. 8 (a). It is worth noting that, the average convection coefficient ($\overline{h}$) is identified as:

$$\overline{h} = \frac{q_{tot}}{(T_{ew} - T_{coolant}) \cdot S} \tag{5}$$

where q_{tot}, T_{ew}, $T_{coolant}$, S are the total heat flux, average temperature of endwinding, average temperature of coolant and contact area between endwinding and coolant.

The convection coefficient for the single layer machine with ferrofluid cooling can be given as an empirical equation such as:

$$y = \mathrm{A} \cdot x^2 - B \cdot x + C \tag{6}$$

where $A = 1.943$, $B = 15.796$, and $C = 89.541$ for this investigation.

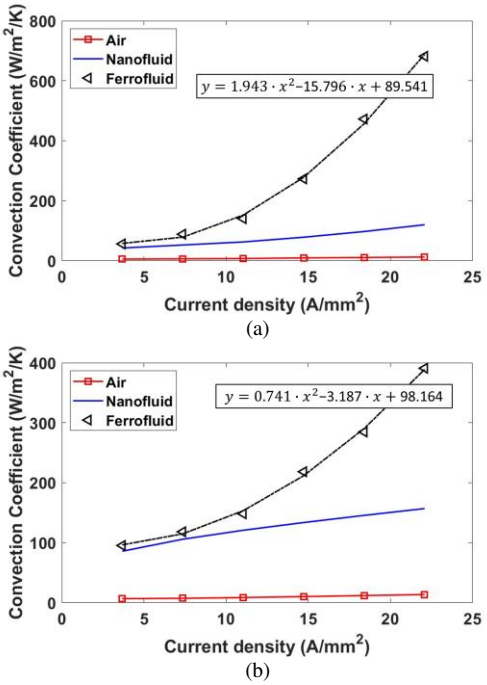

Fig. 8. Average convection coefficient at endwinding surface *vs* current density for different coolants. (a) Single layer and (b) double layer machines.

b. Double layer windings

The same models have also been built to simulate the thermal performances of the double layer SPM machine, and the variations of peak winding temperatures obtained by different models are shown in Fig. 6 (b). When NF is replaced by ferrofluid, the winding peak temperature is significantly reduced from 141℃ to 133℃ (obtained by model 1) or 135℃ (obtained by model 2). In addition, similar to the single layer machine, the difference between the winding temperatures obtained by models 1 and 2 for the double layer machine is only 1.5%, which is also negligible. However, model 1 cannot well estimate the coolant velocity for the double layer machine as shown in Fig. 9 (c) and (d). Appendix B indicates that $\boldsymbol{K}_{(R)}$ is lower than 1 in most regions of the end space for the double layer machine, as shown in Fig. 14. Model 1, which identifies $\boldsymbol{K}_{(R)}$ as 1, overestimates the magnetic body force, resulting in higher coolant velocity in most end-space regions of the double layer machine, as shown in Fig. 9 (c) and (d). This inevitably leads to an overestimation of the cooling efficiency.

It is also found that, the temperature reduction in the double layer machine (8℃ and 6℃ using models 1 and 2) is lower than that of the single layer design (13℃ and 15℃ using models 1 and 2). This is mainly because the number of turns per coil of the double layer winding is half of that of the single layer winding. This leads to a lower magnetic field strength (see Fig. 10) in the end space of the double layer machine. The lower value and smaller gradient of magnetic field strength lead to

lower magnetic body force for the double layer machine. Therefore, the fluid velocity for the double layer machine is lower than that of the single layer counterpart, as shown in Fig. 9. The simulation results reveal that the single layer machine benefits more from the ferrofluid cooling system due to its more significant thermomagnetic convection.

Similar to the single layer machine, the cooling efficiency of ferrofluid for the double layer machine will also be improved when the electrical loading increases. As shown in Fig. 5 (b), the thermomagnetic effect is also more significant when the current density increases. Using ferrofluid to replace nanofluid can improve machine temperature reduction from 8 ℃ (@ 18.4A/mm^2) to 20℃ (@ 22.1A/mm^2). The average convection coefficients at endwinding surfaces for double layer machine with different cooling methods are shown in Fig. 8 (b). The convection coefficient for the double layer machine with ferrofluid cooling can be given as an empirical equation such as:

$$y = A \cdot x^2 - B \cdot x + C \qquad (7)$$

where $A = 0.741$, $B = 3.187$, and $C = 98.164$ for this investigation.

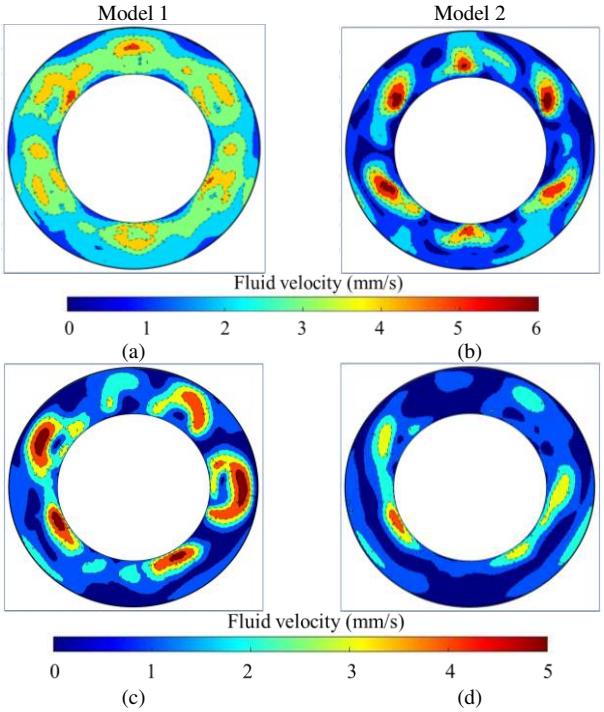

Fig. 9. Fluid flow velocity at plane 1 simulated by (a, c) model 1 and (b, d) model 2 for (a, b) single and (c, d) double layers with ferrofluid cooling.

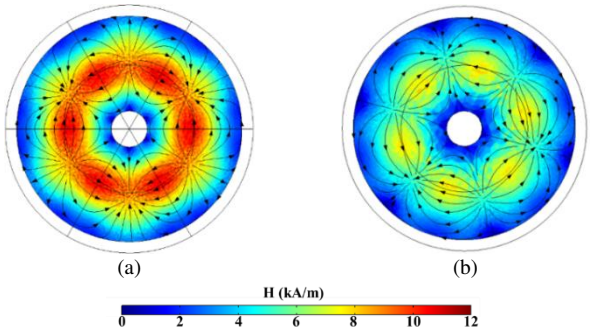

Fig. 10. Magnetic field strength distribution at plane 1 simulated by model 1 for (a) single layer machine and (b) double layer machine at plane 1.

IV. Experimental Validations

A. Test Rig Setup

In order to validate the multiphysics models, a motorette has been built, as shown in Fig. 11 (a). The specifications of this motorette are listed in Table III. An epoxy resin is used to fill the gaps between conductors, as well as the gap between the stator wall and the winding. This helps improve the equivalent thermal conductivity in the stator slots and reduce the uncertainty in thermal modelling. The thermal conductivity and density of this epoxy resin are 0.28 W/m · K and 1160 kg/m^3, respectively. A ferrofluid called STG 1010B manufactured by Ferrotec Corporation has been used for the tests, and its properties are listed in Table IV. The water jacket is located at the back of the motorette as shown in Fig. 11 (a). A commercial pump that can supply 1 L/min inlet flow rate to the water jacket is used for the tests.

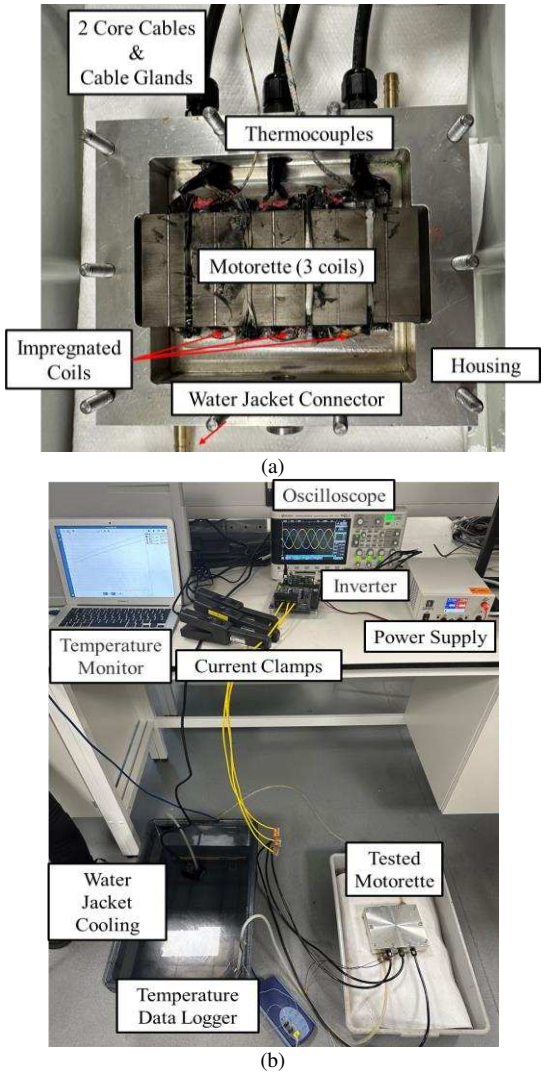

Fig. 11. (a) Tested motorette and (b) test rig.

Table III Specification of Tested Motorette

Stator width (mm)	121	Housing width (mm)	151
Stator active length (mm)	50	Housing axial length (mm)	130
Stator depth (mm)	21.5	Housing depth (mm)	26.5
Slot depth (mm)	15.8	Housing inner length (mm)	100
Slot width (mm)	18.1	Number of turns per coil	33
Slot number	4	Slot fill factor	0.34

TABLE IV PARAMETERS OF THE FERROFLUID (Fe_3O_4)

Saturation magnetization (mT)	11	Dynamic viscosity (Pa · s)	0.1
Thermal conductivity (W/m · K)	0.15	Initial permeability (at 30Oe)	1.68
Thermal expansion coefficient ($\times 10^{-4}$ 1/K)	7.5	Electrical resistivity (Ω/cm)	$> 10^9$
Density at 25℃(kg/m^3)	940	Heat capacity (J/kg/K)	1700

B. Temperature Measurement

3D multiphysics simulations have been carried out and will be compared against the measurements in this section. In the multiphysics models, the ambient temperature is set to be 20℃ and the convection coefficient on the surfaces of the motorette is 8 W/m^2/K. It is worth noting that, based on Hashin and Shtrikman approximation, the corresponding equivalent thermal conductivities of the windings are 0.39 W/m/K and 68.8 W/m/K in the directions that are perpendicular and parallel to the current, respectively.

An 8A dc current is first injected into all coils of the motorette for both the simulations and experiments. To reveal the importance of the model 2, simulations and experiments with ac currents, which have different frequencies but the same rms current (8A), have also been carried out. As expected, for oil cooling, the machine temperatures, specifically the active coil temperature where the thermal couple is located, are almost independent of current supply, i.e., the dc and ac currents (with different frequencies) have almost the same temperatures, as shown in Fig. 12. This also means that the ac losses can be neglected for the tested motorette. Furthermore, the machine temperature is reduced from 63.3℃ (oil) to 61.2℃ (FF @50Hz ac current supply) and 60.9℃ (FF@100Hz ac current supply). By contrast, when a dc current is supplied, the temperature is reduced to 59.8℃ (FF).

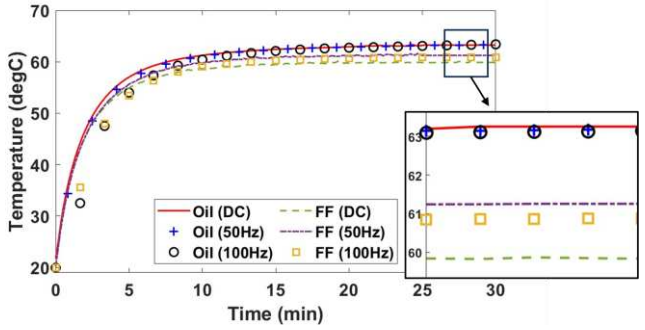

Fig. 12. Measured temperatures *vs* time for both oil and ferrofluid cooling with different current supplies.

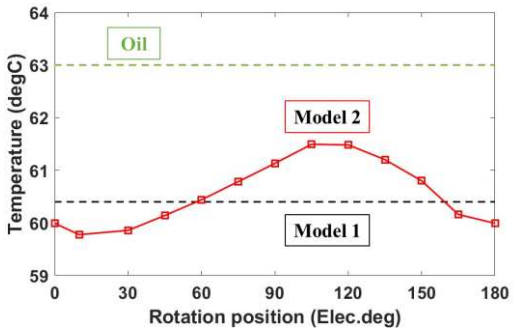

Fig. 13. Simulated temperatures *vs* rotor position for oil and FF cooling. The simulations correspond to the measurements in Fig. 12.

TABLE V SIMULATED AND MEASURED RESULTS WITH DIFFERENT COOLANTS.

Coolant	Simulated (℃)	Measured (℃)	Difference
Oil	63.0	63.3	0.47%
Ferrofluid (DC)	60.4 (Model 1)	59.8	1%
Ferrofluid (AC)	60.6 (Model 2)	61.2 (50Hz)	0.98% (50Hz)
		60.9 (100Hz)	0.5% (100Hz)

Simulations corresponding to the measurements in Fig. 12 have been carried out. It is worth noting that these simulations are only steady-state, as the transient state simulations would be excessively time-consuming. In addition, for FF cooling, both model 1 and model 2 have been used, as shown in Fig. 13. The simulated results shown in Fig. 13 have been compared against the measured results, which are listed in Table V. A generally good agreement can be observed between the simulated and measured results, proving the accuracy of the multiphysics models developed in this paper.

Both measured and simulated results demonstrated that, compared to oil cooling, using ferrofluid as coolant in the end-winding regions can reduce the machine temperature. This is the case for both ac and dc current supplies. Simulated results also demonstrate that, using magnetic field generated by dc current overestimates the ferrofluid cooling efficiency for the double layer machine. This conclusion has also been observed during the experiments. For example, when oil is replaced by ferrofluid as coolant, for the ac current supply, the motorette's temperature is reduced by around 2.1℃, but this reduction is 3.5℃ for the dc current supply. In addition, model 2 cannot fully consider the influence of the frequency of the ac current. However, according to the measured results, this limitation might not be an issue, as the temperature difference between the 50Hz and 100Hz ac currents is negligibly small.

V. CONCLUSION

In this paper, an advanced cooling technology that uses ferrofluid to fill in the end-space of the single layer and double layer machines has been investigated. According to simulation results obtained from 3D multiphysics models, the ferrofluid cooling can significantly reduce the peak temperatures of both the investigated machines. This is because, firstly, ferrofluid has higher thermal conductivity and density than air, which results in a more significant gravitational effect. This contributes to a 5℃ temperature reduction for the single layer machine and a 17℃ temperature reduction for the double layer machine. Secondly, ferrofluid also experience magnetic body force produced by end-winding leakage flux. This thermomagnetic effect drives the coolant circulation between the housing and the end-windings. For the single layer machine, the temperature reduction due to the thermomagnetic effect is around 13℃. However, for the double layer machine, it is around 8℃. The efficiency of the ferrofluid cooling will be more pronounced when the electrical loading increases. A motorette has been built and the multiphysics simulations have been validated by experiments.

VI. APPENDIX

According to lumped-parameter magnetic circuit, the position dependent magnetic field strength ($\boldsymbol{H}_{(R)}$) generated by

only one winding is proportional to the current carried by the winding, and can be derived as

$$\boldsymbol{H}_{(R)} = \boldsymbol{k}_{(R)} I \tag{8}$$

where the index $_R$ represents the location in space, i.e., the distance from the winding carrying current I, and $\boldsymbol{k}_{(R)}$ is a constant which is related to material's permeability and the distance from the winding.

For electrical machines with a total number of n windings, the magnetic field at specific locations in space is

$$\boldsymbol{H}_{(R)} = \sum_{i=1}^{n} \boldsymbol{k}_{i(R)} I_i \tag{9}$$

It is worth noting that $\boldsymbol{H}_{(R)}$ is the magnetic field generated by the windings only (without consideration of PMs). Since the study is focused on end-winding region, the magnetic field generated by the rotating PMs can be neglected.

For machines with a 3-phase AC supply, the magnetic field strength generated by the windings can be rewritten as

$$\boldsymbol{H}_{(R)} = I_{ac} \cdot \sqrt{\boldsymbol{a}_{(R)}^2 + \boldsymbol{b}_{(R)}^2} \cdot \sin\left(2\pi f t + \vartheta_{(R)}\right) \tag{10}$$

where $\boldsymbol{a}_{(R)}$, $\boldsymbol{b}_{(R)}$ and $\vartheta_{(R)}$ are position dependent constants, which are functions of $\boldsymbol{k}_{(R)}$.

Using (1), (3) and (10), the magnetic body force is derived as

$$\boldsymbol{F}_{m(R)} = \mu_0 \chi^2 I_{ac}^2 \nabla\left\{\left[\boldsymbol{a}_{(R)}^2 + \boldsymbol{b}_{(R)}^2\right] \cdot \sin^2\left(2\pi f t + \vartheta_{(R)}\right)\right\} \tag{11}$$

If the machines operate under DC with a current of I_{dc}, $\boldsymbol{H}_{(R)\_dc}$ and $\boldsymbol{F}_{m(R)\_dc}$ are derived as

$$\boldsymbol{H}_{(R)\_dc} = I_{dc} \cdot \boldsymbol{c}_{(R)} \tag{12}$$

$$\boldsymbol{F}_{m(R)\_dc} = \mu_0 \chi^2 I_{dc}^2 \nabla \boldsymbol{c}_{(R)}^2 \tag{13}$$

where $\boldsymbol{c}_{(R)}$ is also a position dependent constant, same as $\boldsymbol{a}_{(R)}$ and $\boldsymbol{b}_{(R)}$. Comparing (11) and (13), the magnetic body force for AC and DC can be equal when

$$I_{dc} = \frac{I_{ac}}{\sqrt{2}} \cdot \boldsymbol{K}_{(R)} \tag{14}$$

where the position dependent coefficient $\boldsymbol{K}_{(R)}$ is

$$\boldsymbol{K}_{(R)} = \frac{\sqrt{\boldsymbol{a}_{(R)}^2 + \boldsymbol{b}_{(R)}^2}}{\boldsymbol{c}_{(R)}} \tag{15}$$

A. Model 1

For the electrical machines with windings that are relatively far apart, for example, the single layer windings, the magnetic field is mostly generated by each winding itself without too much mutual flux from the adjacent windings, $\boldsymbol{H}_{(R)}$ in (9) can be simplified as

$$\boldsymbol{H}_{(R)} = \boldsymbol{k}_{j(R)} I_j \tag{16}$$

where j denotes the adjacent winding. Therefore, the position dependent constants can be rewritten as

$$\begin{cases} \boldsymbol{a}_{(R)} = \boldsymbol{c}_{(R)} = \boldsymbol{k}_{j(R)} \\ \boldsymbol{b}_{(R)} = \vartheta_{(R)} = 0 \\ \boldsymbol{K}_{(R)} = 1 \end{cases} \tag{17}$$

Since $\boldsymbol{K}_{(R)} = 1$, (14) can be re-written as

$$I_{dc} = I_{ac}/\sqrt{2} \tag{18}$$

The equation (18) demonstrates that for single layer machines, a DC value equivalent to the rms value of an AC can generate a magnetic body force similar to that of the AC.

B. Model 2

For the electrical machines with windings that are close to each other, for example, the double layer windings or integer slot overlapping windings, the magnetic field is often generated by several windings. In such case, (16) is not accurate enough. A coefficient $\boldsymbol{K}_{(R)}$ is needed to obtain a more accurate distribution of magnetic body force. To calculate $\boldsymbol{K}_{(R)}$ in the end-space, 3D FEM (COMSOL software package) has been used. The results in Fig. 14 show that $\boldsymbol{K}_{(R)}$ at different positions within the end-space of the double layer machine is significant. It is also worth noting that, the blank region, mostly located in the center between two adjacent windings, means that $\boldsymbol{K}_{(R)}$ is larger than 1. This also means that it is impossible to make the magnetic field at each location within the end-space the same for the DC and AC supplies if a single DC excitation is used.

To address this issue, a new model (model 2) with 3-phase excitation but each phase is injected with a different DC current to simulate the AC current supply is proposed. With this kind of current supply, at each rotor position, the steady-state temperatures at different locations within the machine will be obtained. Then these temperatures (at each location within the machine) for different rotor positions will be averaged to work out the temperature distribution that is similar to a real 3-phase AC currents supply.

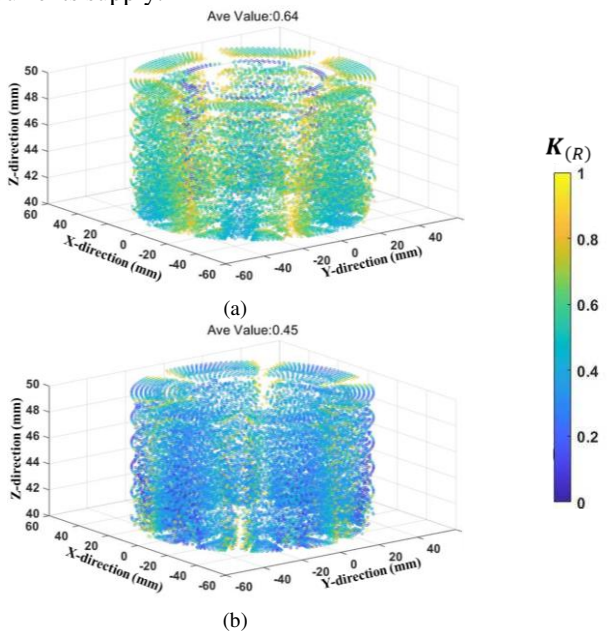

Fig. 14. $K_{(R)}$ (a) in radial and (b) tangential directions within the end-space of the double-layer machine. Z-direction is along the machine's rotation axis.

Acknowledgement

For the purpose of open access, the author has applied a Creative Commons Attribution (CC BY) licence to any Author Accepted Manuscript version arising.

VII. REFERENCE

[1] V. Montsinger, "Loading transformers by temperature," *Trans. AIEE,* vol. 49, no. 2, pp. 776-790, Apr. 1930.

[2] M. Popescu, D. Staton, D. Dorrell, F. Marignetti, and D. Hawkins, "Study of the thermal aspects in brushless permanent magnet machines performance," in *2013 IEEE WEMDCD*, Mar. 2013: IEEE, pp. 60-69.

[3] S. Ulbrich, J. Kopte, and J. Proske, "Cooling fin optimization on a TEFC electrical machine housing using a 2-D conjugate heat transfer model," *IEEE Trans. Ind. Electron.,* vol. 65, no. 2, pp. 1711-1718, Sep. 2017.

[4] A. Nollau and D. Gerling, "A flux barrier cooling for traction motors in hybrid drives," in *2015 IEEE IEMDC*, 2015: IEEE, pp. 1103-1108.

[5] A. Tüysüz, F. Meyer, M. Steichen, C. Zwyssig, and J. W. Kolar, "Advanced cooling methods for high-speed electrical machines," *IEEE Trans. Ind. Appl.,* vol. 53, no. 3, pp. 2077-2087, Feb. 2017.

[6] Y. Gai, M. Kimiabeigi, J.D. Widmer, Y. C. Chong, J. Goss, U. SanAndres, D. A. Staton, "Shaft cooling and the influence on the electromagnetic performance of traction motors," in *2017 IEEE IEMDC*, May 2017: IEEE, pp. 1-6.

[7] Y. Gai, D. J. D. Widmer, A. Steven, Y. C. Chong, M. Kimiabeigi, J. Goss, M. Popescu, "Numerical and experimental calculation of CHTC in an oil-based shaft cooling system for a high-speed high-power PMSM," *IEEE Trans. Ind. Electron.,* vol. 67, no. 6, pp. 4371-4380, Jun. 2019.

[8] R. Zhou, G. Li, Z. Zhu, M. Foster, and D. Stone, "Improved cooling in modular consequent pole PM machine utilizing flux gaps," in *2020 IEEE ECCE*, 2020: IEEE, pp. 4253-4260.

[9] Y. C. Chong, E. J. E. Subiabre, M. A. Mueller, J. Chick, D. A. Staton, and A. S. McDonald, "The ventilation effect on stator convective heat transfer of an axial-flux permanent-magnet machine," *IEEE Trans. Ind. Electron.,* vol. 61, no. 8, pp. 4392-4403, Aug. 2013.

[10] Z. Xu, A. La Rocca, P. Arumugam, S. J. Pickering, C. Gerada, S. Bozhko, D. Gerada, H. Zhang, "A semi-flooded cooling for a high speed machine: Concept, design and practice of an oil sleeve," in *43rd Annu. Conf. IEEE Ind. Electron. Soc. (IECON)*, Oct./Nov. 2017: IEEE, pp. 8557-8562.

[11] A. La Rocca, Z. Xu, P. Arumugam, S. J. Pickering, C. N. Eastwick, C. Gerada, S. Bozhko, "Thermal management of a high speed permanent magnet machine for an aeroengine," in *2016 XXII ICEM*, Sep. 2016: IEEE, pp. 2732-2737.

[12] F. Wu and A. M. EL-Refaie, "Additively manufactured hollow conductors with integrated cooling for high specific power electrical machines," in *2020 ICEM*, Aug. 2020, vol. 1: IEEE, pp. 1497-1503.

[13] C. Micallef, S. J. Pickering, K. A. Simmons, and K. J. Bradley, "An alternative cooling arrangement for the end region of a totally enclosed fan cooled (TEFC) induction motor," *Proc. 4th IET Conf. PEMD,* 2008.

[14] M. Kang, H. Wang, L. Guo, T. Shi, and C. Xia, "Self-circulation cooling structure design of permanent magnet machines for electric vehicle," *Appl. Therm. Engin.,* vol. 165, p. 114593, Jan. 2020.

[15] M. Polikarpova, P. Lindh, J. Tapia, and J. Pyrhönen, "Application of potting material for a 100 kW radial flux PMSM," in *2014 ICEM*, Sep. 2014: IEEE, pp. 2146-2151.

[16] Y. Sun, S. Zhang, W. Yuan, Y. Tang, J. Li, and K. Tang, "Applicability study of the potting material based thermal management strategy for permanent magnet synchronous motors," *Appl. Thermal Eng.,* vol. 149, pp. 1370-1378, Feb. 2019.

[17] W. Lian, Y. Xuan, and Q. Li, "Characterization of miniature automatic energy transport devices based on the thermomagnetic effect," *Energy Conv. manag.,* vol. 50, no. 1, pp. 35-42, Jan. 2009.

[18] V. Segal and K. Raj, "An investigation of power transformer cooling with magnetic fluids," *Indian J. Eng. Mater. Sci.,* 1998.

[19] L. Pîslaru–Dănescu, A. M. Morega, M. Morega, V. Stoica, O. M. Marinică, F. Nouraş, N. Păduraru, I. Borbáth, T. Borbáth, "Prototyping a ferrofluid-cooled transformer," *IEEE Trans. Ind. Appl.,* vol. 49, no. 3, pp. 1289-1298, 2013.

[20] R. Zanella, C. Nore, F. Bouillault, J. L. Guermond, and X. Mininger, "Influence of thermomagnetic convection and ferrofluid thermophysical properties on heat transfers in a cylindrical container heated by a solenoid," *J. Magn. Magn. Mater.,* vol. 469, pp. 52-63, Jan. 2019.

[21] G. Karimi-Moghaddam, R. D. Gould, S. Bhattacharya, and D. D. Tremelling, "Thermomagnetic liquid cooling: A novel electric machine thermal management solution," in *2014 IEEE ECCE*, Sep. 2014: IEEE, pp. 1482-1489.

[22] W. Zhang, G. Li, B. Ren, Y. Chong, and M. Michon, "Investigation of Ferrofluid Cooling for High Power Density Permanent Magnet Machines," *IEEE Transactions on Magnetics,* vol. 59, no. 1, pp. 1-11, 2022.

[23] R. E. Rosensweig, *Ferrohydrodynamics*. Mineola, N.Y.: Dover Publications, 1997.

[24] J. Patel, K. Parekh, and R. Upadhyay, "Prevention of hot spot temperature in a distribution transformer using magnetic fluid as a coolant," *Int. J. Therm. Sci.,* vol. 103, pp. 35-40, May 2016.

[25] S. N. El Dine, X. Mininger, C. Nore, R. Zanella, F. Bouillault, and J.-L. Guermond, "Impact of Magnets on Ferrofluid Cooling Process: Experimental and Numerical Approaches," *IEEE Trans. Magn.,* vol. 56, no. 1, pp. 1-4, Dec. 2019.

[26] T. H. Boyer, "The force on a magnetic dipole," *American J. Phys.,* vol. 56, no. 8, pp. 688-692, Aug. 1988.

[27] Y. Aharonov and A. Casher, "Topological quantum effects for neutral particles," *Phys. Rev. Lett.,* vol. 53, no. 4, p. 319, Jul. 1984.

[28] L. Cecchini and A. Chiolerio, "The magnetic body force in ferrofluids," *J. Phys. D: Appl. Phys.,* vol. 54, no. 35, p. 355002, Jun. 2021.

[29] B. Berkovsky, V. F. Medvedev, and M. S. Krakov, *Magnetic fluids: engineering applications*. New York, USA: Oxford Univ, 1993.

[30] H. Hezaveh, A. Fazlali, and I. Noshadi, "Synthesis, rheological properties and magnetoviscos effect of Fe2O3/paraffin ferrofluids," *J. Taiwan Inst. Chem. Engin.,* vol. 43, no. 1, pp. 159-164, 2012.

Wei Zhang received the B.Eng. degrees in Faculty of Science and Engineering from Communication University of China, Beijing, China, in 2018, the M.Sc. degree in electrical and electronic engineering from the University of Sheffield, Sheffield, UK, in 2019. Since 2019, he has been working toward the Ph.D. degree in electrical and electronic engineering at the University of Sheffield, Sheffield, U.K. His research interests include the electromagnetic design, fluid dynamics analysis, and thermal management of electrical machines.

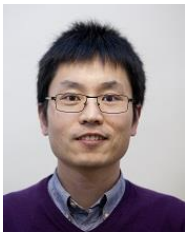

Guang-Jin Li (M'10–SM'16) received the bachelor's degree from Wuhan University, China, in 2007, the master's degree from the University of Paris XI, France, in 2008, and the PhD degree from the Ecole Normale Supérieure (ENS) de Cachan, Paris, France, in 2011, all in electrical and electronic engineering. He joined the Electrical Machines and Drives (EMD) Group, University of Sheffield, Sheffield, U.K., in June 2012, as a Postdoctoral Research Associate, where he was appointed as an Assistant Professor, in September 2013, and promoted to Associate Professor in January 2018 and Professor in January 2022. His main research interests include the design, fault diagnostics, and thermal management of electrical machines for renewable energy, automotive, and electrical aircrafts.

Ying Qin (Student Member, IEEE) received the B.Eng. and M.Sc. degrees in electrical engineering from JiangSu University, Zhenjiang, China, in 2012 and 2015, respectively. From 2015 to 2018, he was an Engineer with the SAIC Motor Ltd., Shanghai, China. From 2018 to 2020, he was a Senior Engineer with Delta Electronics Company Ltd., Shanghai, China. Since 2020, he has been working toward the Ph.D. degree at the University of Sheffield, Sheffield, U.K. His research interests include power-electronics, control of electric machines, electrical machine fault modeling, machine fault detection, and fault-tolerant drives.